AIAA JOURNAL
Vol. 42, No. 6, June 2004

Technical Notes

TECHNICAL NOTES are short manuscripts describing new developments or important results of a preliminary nature. These Notes cannot exceed six manuscript pages and three figures; a page of text may be substituted for a figure and vice versa. After informal review by the editors, they may be published within a few months of the date of receipt. Style requirements are the same as for regular contributions (see inside back cover).

Turbulent Energy Balances Inside Short Bubble Formed on NACA 0012 Airfoil

Kenichi Rinoie* and Koi Hata†
University of Tokyo, Tokyo 113-8656, Japan

Introduction

AFTER the laminar boundary layer separates from the airfoil surface, the flow can reattach to the surface as a turbulent shear layer. This region between the laminar separation and the reattachment is called a laminar separation bubble.[1] The laminar separation bubble on the airfoil is classified into a short bubble and a long bubble. A short bubble abruptly fails to reattach to the airfoil surface when the airfoil angle of attack is increased, which is known as a short bubble burst and is the cause of airfoil stall. After the burst, a long bubble is formed. The turbulent flow developed inside of the short bubble plays a crucial role in both formation and maintenance of the bubble.[1] Detailed knowledge of the turbulence inside the short bubble is essential to understand its behavior. However, presently available experimental data of the laminar separation bubble are very few.[2,3]

Turbulent energy balance is a methodology that can assist in the understanding of the turbulent flow structure and has been successfully used to discuss the separated and reattaching flow formed over a backward-facing step.[4,5] In Ref. 3, the turbulent energy balance analysis has also been conducted for the short bubble formed on a NACA 63-009 airfoil at the angle of attack α of 7 deg and at the chord Reynolds number of 8.3×10^4. It was concluded that the turbulent energy production has the largest contribution to the turbulence growth. However, because the measurements were conducted by the use of one-component laser Doppler anemometry (LDA) and by rotation of the LDA optics around the laser beam axis at each measuring point to acquire the two-dimensional velocity components, it is thought that the results contain relatively high measurement errors. In this Note, therefore, the turbulent energy balance analysis has been conducted based on the experimental results[6] of a short bubble formed on a NACA 0012 measured with a two-component LDA. The purpose of the present Note is to provide basic information and data of turbulence development inside the short bubble.

Received 12 May 2003; revision received 21 July 2003; accepted for publication 22 July 2003.

*Associate Professor, Department of Aeronautics and Astronautics, School of Engineering, 7-3-1 Hongo, Bunkyo-ku. Senior Member AIAA.

†Graduate Student, Department of Aeronautics and Astronautics, School of Engineering, 7-3-1 Hongo, Bunkyo-ku.

Experimental Methods and Results

In this section, experimental methods and results are briefly summarized. Reference 6 investigated the short bubble formed on the NACA 0012 airfoil at a Reynolds number of 1.3×10^5 based on the chord length ($c = 200$ mm) and at an angle of attack α of 10 deg. The wind tunnel (width 200 mm), the two-component LDA, and the LDA measuring methodology are the same as those used in Ref. 5, and details are described in this reference.

Mean velocities ($\bar{U}$, $\bar{V}$), turbulent stresses ($\overline{u^2}$, $\overline{uv}$, $\overline{v^2}$), and turbulent triple products ($\overline{u^3}$, $\overline{u^2v}$, $\overline{uv^2}$, $\overline{v^3}$) defined in the freestream coordinate (x, y) were measured. The number of burst samples for each measurement was set at 10,000, with a sampling data rate of about 3000 Hz. The estimated overall accuracy is $\pm 2\%$ for mean velocity, $\pm 2.5\%$ for turbulent stresses, and $\pm 6\%$ for turbulent triple products at 20:1 odds when $\bar{U} = 0.8U_\infty$ and $\sqrt{\overline{u^2}}/U_\infty = 0.23$ (where U_∞ is freestream velocity). A method similar to that in Ref. 5 was used to estimate the uncertainty values of beam alignment, resolution of the signal processor, and statistical uncertainties.[7] A transit time weighting method[8] was used to eliminate velocity bias errors. The positioning accuracy of the measurement volume is better than ± 0.1 mm. The surface pressure measurements indicated that the short bubble burst occurs between $\alpha = 11$ and 11.5 deg. LDA measurements were made at $\alpha = 10$ deg, when the short bubble is formed. A surface oil-flow visualization test was made to confirm the two dimensionalities of the mean flow at the tunnel centerline at $\alpha = 10$ deg.

Distribution of mean velocity profiles with local flow direction are shown in Fig. 1a. A dividing streamline starting from the laminar separation point, which is defined as a contour of a stream function,

$$\psi \equiv \int_0^y \bar{U}\,dy = 0$$

is also shown. The reattachment point is at about $x_c/c = 0.1$ (where x_c is a coordinate along the airfoil chordline measured from the leading edge). Figure 1b shows turbulent stress distributions. The turbulent stresses start to increase after the laminar separation takes place. After the transition, the level of the turbulent intensity grows and the flow reattaches to the surface.

Turbulent Energy Balances

The turbulent energy balances were estimated from the following transport equations of the turbulent energy k, as in Refs. 3 and 5:

$$0 = -\left(\bar{U}\frac{\partial k}{\partial x} + \bar{V}\frac{\partial k}{\partial y}\right) - \overline{uv}\left(\frac{\partial \bar{U}}{\partial y} + \frac{\partial \bar{V}}{\partial x}\right) - \left(\overline{u^2}\frac{\partial \bar{U}}{\partial x} + \overline{v^2}\frac{\partial \bar{V}}{\partial y}\right) - \frac{\partial}{\partial x}\overline{uk} - \frac{\partial}{\partial y}\overline{vk} - \varepsilon \tag{1}$$

The mean flow is assumed to be two dimensional and the turbulence is steady. The turbulent energy $k = \frac{1}{2}\cdot(\overline{u^2} + \overline{v^2} + \overline{w^2})$ was approximated by $\frac{3}{4}\cdot(\overline{u^2} + \overline{v^2})$ by the assumption that the spanwise turbulent stress $\overline{w^2}$ is about the same magnitude as other types of turbulent stresses ($\overline{u^2}$, $\overline{v^2}$). Diffusions by pressure fluctuation

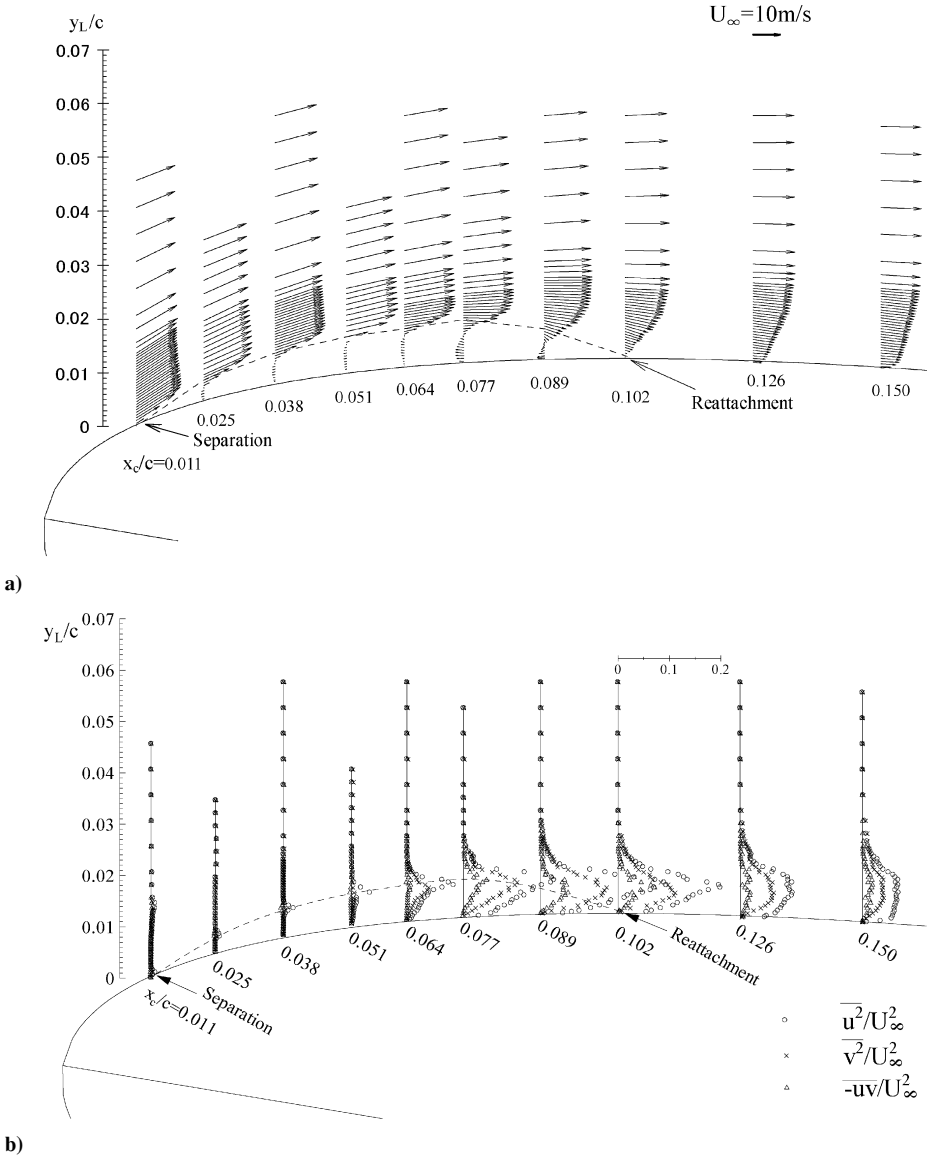

Fig. 1 Experimental results[6]: a) mean velocity profiles and b) turbulent stress profiles (y_L, local coordinate perpendicular to x and measured from the airfoil surface at each x_c).

p and viscosity cannot be evaluated. Dissipation ε in Eq. (1) was evaluated as the difference of all of the other terms; therefore, effects of diffusions by pressure fluctuation and viscosity are also included in this term. All terms were made dimensionless by U_∞^3/c.

Figures 2a and 2b show balances of turbulent kinetic energy k at two chordwise stations upstream of reattachment and Fig. 2c that very near reattachment. In Fig. 2a, at the chordwise station of $x_c/c = 0.077$, where the maximum reverse flow velocity is observed in Fig. 1a, the largest contribution to the growth of the turbulent energy is the production by shear stress $-\overline{uv}(\partial\bar{U}/\partial y + \partial\bar{V}/\partial x)$. The maximum value of this term is attained at the central part of the separated shear layer. One of the secondary dominant terms is dissipation $-\varepsilon$. The transverse diffusion $-\partial\overline{vk}/\partial y$ is another secondary dominant term and is negative at the central part of the shear layer and positive at the outer part, as well as near the surface. The turbulent energy produced at the center of the shear layer is diffused to the upper and lower parts of the layer. Production by normal stress $-\overline{u^2}\partial\bar{U}/\partial x - \overline{v^2}\partial\bar{V}/\partial y$ at the center of the shear layer shows a positive value at the central part of the shear layer, as does the production by shear stress.

From the examples of balances upstream from the reattachment ($x_c/c = 0.089$; Fig. 2b) and near the reattachment ($x_c/c = 0.102$; Fig. 2c), it can be seen that the distribution of each term is qualitatively the same as in Fig. 2a. As the shear layer develops and approaches reattachment, the y position where each term has its peak value moves toward the airfoil surface. These features of production, diffusion, and dissipation terms shown in Fig. 2 are relatively similar to the results of the short bubble in Ref. 3.

Integrals Along a Constant Chordwise Station

Each term in the turbulent energy balance across the entire measured region at a constant chordwise station was integrated and is plotted against the chordwise station as in Refs. 3 and 5. Results are shown in Fig. 3a. Each term is made dimensionless by U_∞^3. Productions by shear stress and those by normal stress are added and plotted as one term. Transverse and longitudinal diffusions are also added and plotted as one term. The maximum values of turbulent energy at each chordwise station $k_{\max}$ are also plotted. The dominant term in the turbulent energy balance is production. The diffusion has a value that is almost zero as a consequence of the integrals. The distribution of the production term is relatively similar to that of $k_{\max}$.

A similar analysis was conducted for the short bubble formed on the NACA 63-009 (Ref. 3). The results are shown in

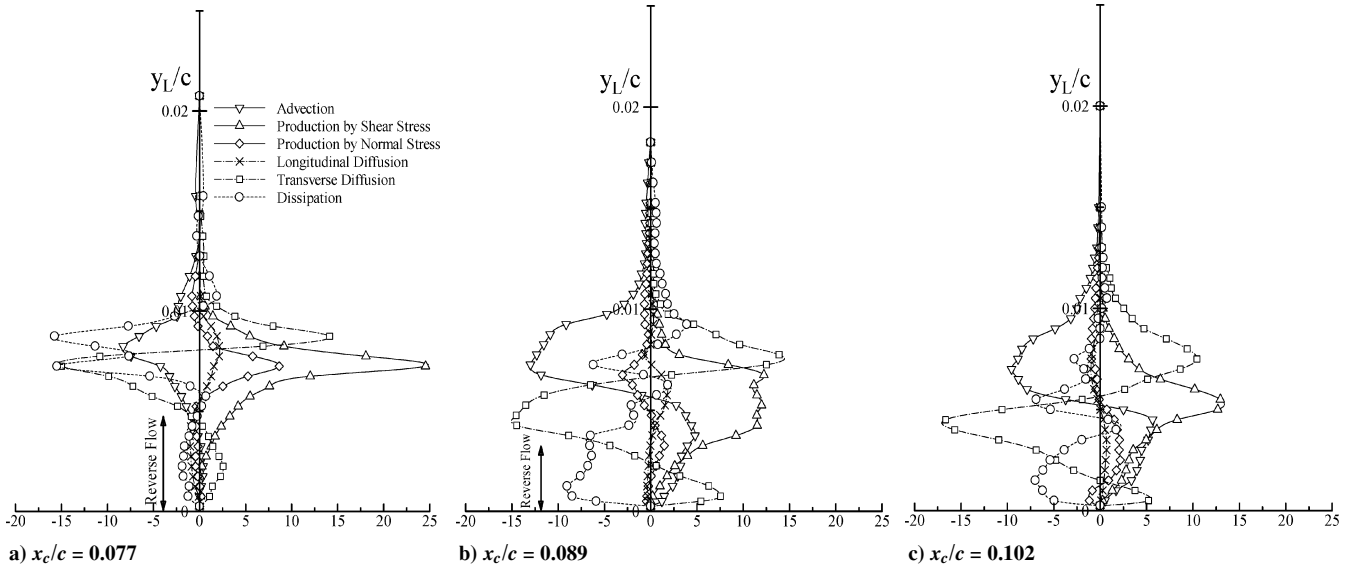

Fig. 2 Turbulent energy balances.

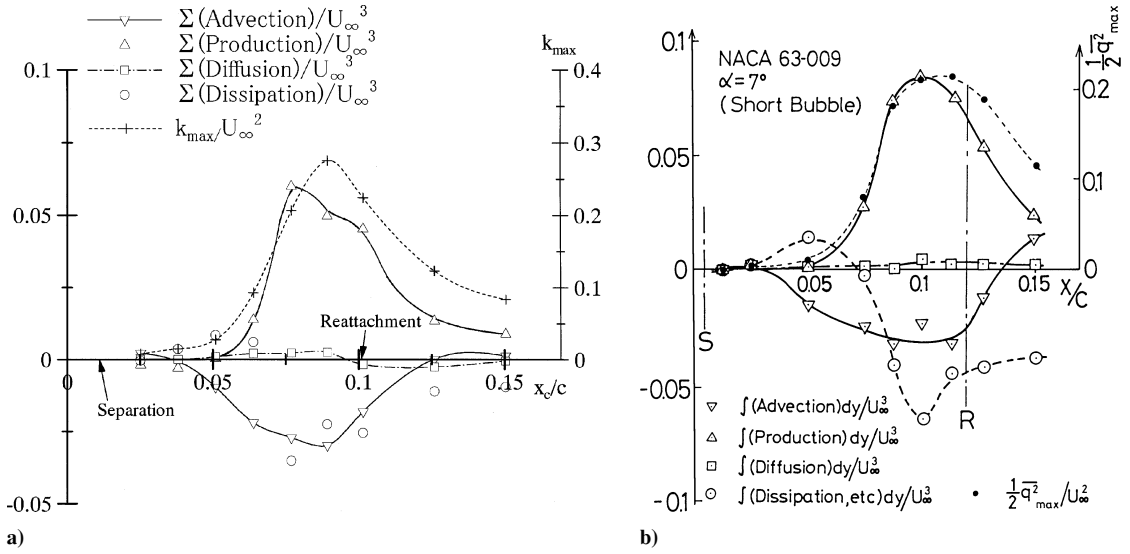

Fig. 3 Integrals of turbulent energy balances along *y* direction: a) NACA 0012, α = 10 deg ($Re_c = 1.3 \times 10^5$) and b) NACA 63-009, α = 7 deg ($Re_c = 8.3 \times 10^4$) (from Ref. 3) ($\frac{1}{2}\overline{q^2}$, turbulent energy *k*).

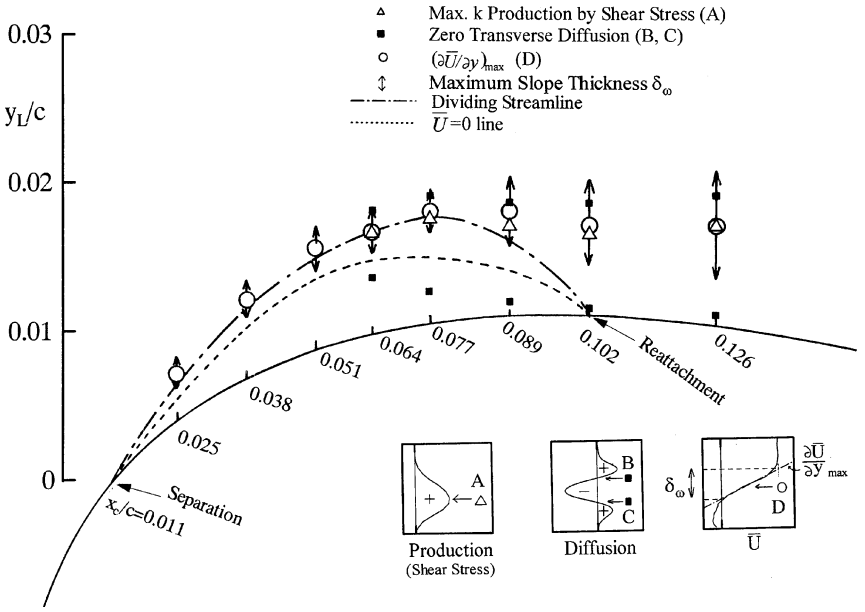

Fig. 4 Spatial distributions of turbulent energy balance; effects of production by shear stress and transverse diffusion.

Fig. 3b. Each term in Fig. 3a and 3b distributes quite similarly. For both short bubbles, the production term attains its maximum and begins to decrease well before the reattachment.

Spatial Distributions

In Fig. 4, the points where the production by shear stress $[-\overline{uv}(\partial\bar{U}/\partial y + \partial\bar{V}/\partial x)]$ reaches its maximum (point A in Fig. 4) and where the transverse diffusion term $(-\partial\overline{vk}/\partial y)$ changes its sign, that is, zero diffusion points, points B and C, are shown. The position where the gradient of the mean longitudinal velocity, $\partial\bar{U}/\partial y$, reaches its maximum (point D) and the maximum slope thickness δ_ω are also plotted in Fig. 4 to indicate the shear layer growth. The same method discussed regarding spatial distributions in Fig. 4 was used in Ref. 5. The maximum slope thickness, which is a measure of the shear layer growth, is defined by $\delta_\omega \equiv \overline{U_e}/(\partial\bar{U}/\partial y)_{\max}$, where $\overline{U_e}$ denotes the maximum $\bar{U}$ for each chordwise station. Distributions of δ_ω are indicated by $\updownarrow$ in Fig. 4. The vertical scale is enlarged for clarity.

The chordwise distributions of the maximum production points A and maximum velocity gradient points D almost coincide. The distance between the zero diffusion points (B and C) increases toward the reattachment. As this distance increases, the thickness of the shear layer also grows toward the reattachment, which indicates the effects of turbulent diffusion. However, this growth is located outside of the reverse flow region.

Conclusions

In summary, results of the short bubble formed on the NACA 0012 indicate that the production term has the largest contribution to the growth of turbulent energy that coincides with those of the short bubble formed on NACA 63-009. The present results also indicate that the width of the separated shear layer increases toward the reattachment due to the effects of transverse diffusion. The results for this Note were measured more accurately than those previously measured for a NACA 63-009 using and can be used as basic information and data for turbulent developments inside a short bubble.

References

[1]Tani, I., "Low-Speed Flows Involving Bubble Separation," *Progress in Aeronautical Sciences*, Vol. 5, Pergamon, New York, 1964, pp. 70–103.

[2]Fitzgerald, E. J., and Mueller, T. J., "Measurements in a Separation Bubble on an Airfoil Using Laser Velocimetry," *AIAA Journal*, Vol. 28, No. 4, 1990, pp. 584–592.

[3]Rinoie, K., Shingo, M., and Sato, J., "Measurements of Short Bubble and Long Bubble Formed on NACA 63-009 Airfoil," *Journal of the Japan Society for Aeronautical and Space Sciences*, Vol. 38, No. 436, 1990, pp. 251–257 (in Japanese).

[4]Driver, D. M., and Seegmiller, H. L., "Features of a Reattaching Turbulent Shear Layer in Divergent Channel Flow," *AIAA Journal*, Vol. 23, No. 2, 1985, pp. 163–171.

[5]Rinoie, K., Shirai, Y., and Sunada, Y., "Behavior of Separated and Reattaching Flow Formed over a Backward Facing Step," *Transactions of the Japan Society for Aeronautical and Space Sciences*, Vol. 45, No. 147, 2002, pp. 20–27.

[6]Hata, K., Rinoie, K., Takemura, N., and Sunada, Y., "Experimental Studies of Low Frequency Velocity Disturbances Observed in Short Bubble Formed on Airfoil," *Journal of Japan Society for Aeronautical and Space Sciences*, Vol. 50, No. 582, 2002, pp. 293–300 (in Japanese).

[7]Brunn, H. H., *Hot-Wire Anemometry*, Oxford Univ. Press, Oxford, 1995, pp. 405–445.

[8]Petrie, H. L., Samimy, M., and Addy, A. L., "Laser Doppler Velocity Bias in Separated Turbulent Flows," *Experiments in Fluids*, Vol. 6, No. 2, 1988, pp. 80–88.

W. Devenport
Associate Editor

Experimental Study of a Weak Vortex–Normal Shock Interaction

I. M. Kalkhoran* and C. Paek†
Polytechnic University, Brooklyn, New York 11201

Introduction

INTERACTION of a streamwise vortex with an otherwise normal shock front, commonly called normal shock wave–vortex interaction, constitutes a problem of some importance in supersonic flows. Interactions of this type are commonplace on supersonic aircraft and missiles, where vortices generated by forward components can encounter shock waves in close proximity to wings and control surfaces present in their passages. These interactions are in general undesirable from a performance standpoint because they may lead to loss of lift, increase in drag, and may alter the stability and control characteristics of the vehicle. Another deleterious possibility is the ingestion of streamwise vortices by the air intake system of a supersonic vehicle resulting in decreased engine performance, blockages of the engine intake, or possibly inlet unstart.

Numerous experimental studies of the interaction between isolated streamwise vortices and otherwise normal shock waves have been carried out.[1–5] In summary, the results of these studies have revealed vortex breakdowns for vortex–shock wave combinations exceeding certain strengths. Moreover, both experimental and theoretical studies have indicated an inverse relationship between the vortex strength and the shock wave intensity at breakdown.[6] It is also clear that the interaction structure depends strongly on the methodology used to generate streamwise vortices and, hence, on the distribution of flow properties within vortex cores. In their work, Delery et al.[2] obtained a shock-induced vortex breakdown limit relating a vortex intensity parameter defined by $\tau_{\max} = (V_\theta)_{\max}/V_\infty$ to the strength of the normal shock wave as determined by the freestream Mach number. In a subsequent study, Kalkhoran et al.[5] carried out an experimental study of the interaction of streamwise wing-tip vortices with otherwise planar normal shock fronts at Mach 2.49. These experiments revealed conical vortex distortion patterns possessing many of the visual characteristics of incompressible vortex breakdown. In a later study,[7] these vortex distortions were shown to be distinct forms of vortex breakdown possessing many of the characteristics of the well-documented low-speed vortex breakdown with a region of reversed flow and stagnation points on the vortex axis.

Considering the simplified situation of the interaction between an axisymmetric streamwise vortex and a planar normal shock wave, the axial Mach number of the vortex is significantly reduced from supersonic to subsonic values when crossing the shock. On the other hand, the swirl component of the Mach number, being approximately tangent to the shock surface, is only marginally influenced. Consequently, the swirl ratio of the vortex will significantly increase in crossing the shock front with the jump in the swirl ratio being directly proportional to the strength of the shock, which in turn is determined by the freestream Mach number. This change in the swirl ratio of the vortex must have a significant effect on the stability of the vortex and consequently on the structure of the downstream flow. Generally, vortex breakdown occurs when the swirl ratio reaches a critical value beyond which a coherent vortical

Received 16 May 2003; revision received 8 January 2004; accepted for publication 27 February 2004.

*Associate Professor, Department of Mechanical, Aerospace, and Manufacturing Engineering. Senior Member AIAA.

†Graduate Student, Department of Mechanical, Aerospace, and Manufacturing Engineering.